P9.1

A Study of Convective Initiation Failure on 22 October 2004

Jennifer M. Laflin and Philip N. Schumacher
National Weather Service, Sioux Falls, SD

1. Introduction

Convective initiation in the presence of strong forcing for ascent and large convective inhibition provides a significant forecasting challenge. In many of these cases, the conditional probability of significant severe weather can be high, with the occurrence of convective initiation as the limiting factor. Part of the forecast process involves examining numerical model output, both from models with parameterized convection and more recently, models with convection treated explicitly. In many cases, operational models will indicate that convection is likely; however, initiation does not occur. Therefore, developing an understanding of how convective initiation occurs in models is critical to producing more accurate forecasts. This study will examine a case study in which convective initiation was forecast by all operational models but did not occur.

On the evening of 22 October 2004, a low pressure system moved eastward across portions of the Northern Plains, while an associated dryline developed in eastern Nebraska and lifted northeastward into northwest Iowa. All cycles of the operational models, including the North American Model (NAM), Global Forecast Model (GFS), and Rapid Update Cycle (RUC) forecast convection to initiate along the boundary by 0000 UTC on 23 October 2004 (Figure 1), despite a large capping inversion present on observed soundings during the morning and early afternoon hours (Figure 2).

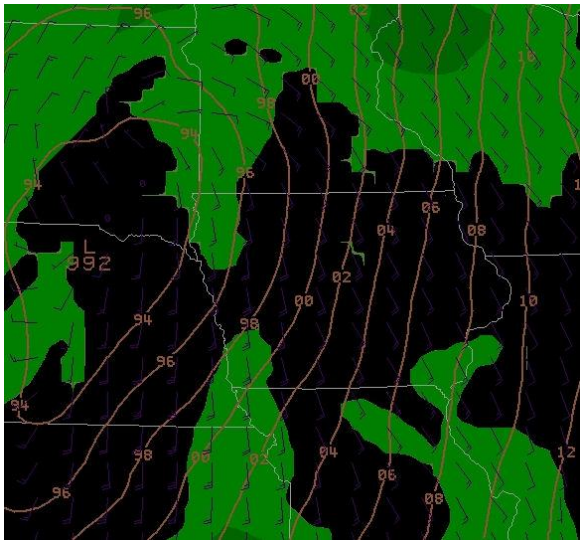

Figure 1. NAM20 precipitation (shaded), wind, and mean sea-level pressure at 00 UTC 23 October.

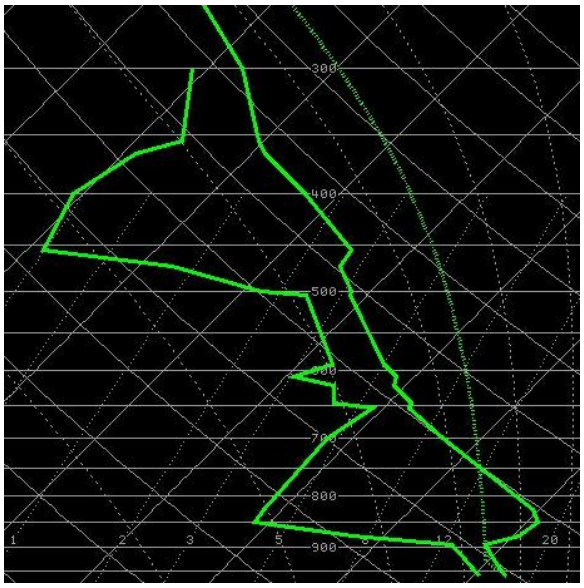

Figure 2. 18 UTC KOAX sounding.

Initially, the forecast models resolved the inversion, but eroded the cap throughout the day (Figure 3). In addition to producing

precipitation, forecast parameters indicated that the environment was favorable for severe convection, which caused an anticipation of severe weather by local offices in the area and by the Storm Prediction Center. However, convection did not initiate along the dryline, resulting in a null event. The purpose of this study is to determine why precipitation did not occur along the dryline, as well as the reason that all three forecast models incorrectly forecast convection. This is done by examining observations, and through model simulations of the event using the Advanced Research Weather Research and Forecasting model (WRF-ARW).

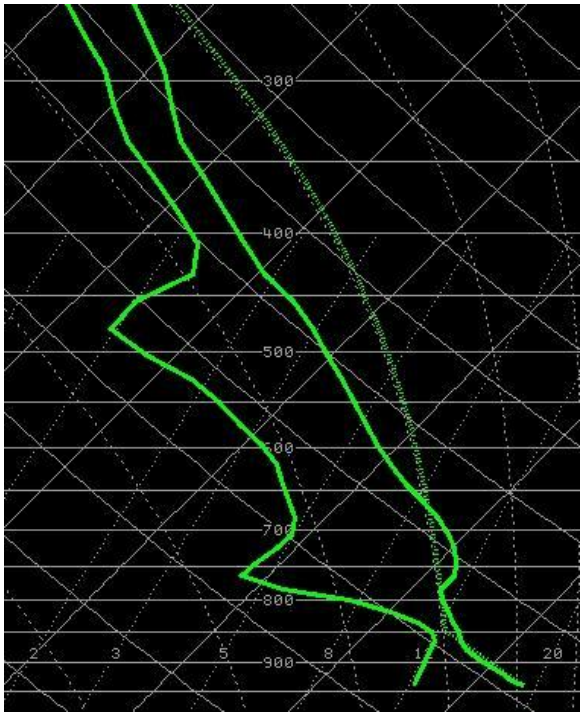

Figure 3. 22 UTC NAM20 sounding for KSPW

A comparison of the WRF-ARW simulations to the forecast models and to a convective-resolving simulation allow for an analysis of how convective parameterizations may affect the model's ability to forecast convective initiation in a capped environment, and how models handle the evolution of capping inversions in the presence of strong low-level forcing for ascent. Results from this study may help to identify the necessity of running a high-resolution local model at National Weather Service offices when convection is forecast by the operational models, and will help forecasters understand how models handle capping inversions so that model failure in short-term convective forecasts can be better anticipated.

2. Data and Methodology

To examine the impact of convective parameterizations on precipitation forecasts, a series of five simulations are conducted. The model used for simulations is the WRF-ARW run locally at the National Weather Service forecasting office in Sioux Falls, SD, and these simulations are initialized with the North American Regional Reanalysis dataset (NARR; Mesinger et al. 2006). All simulations were initialized at 0000 UTC 22 October 2004 and run for 36 hours, which allows 18-24 hours for the model to adjust before the time that convection initiated in the operational models (0000 UTC 23 October; see Figure 1). Operational models that produced convection during the case study event varied in grid spacing from 50 km (GFS) to 20 km (RUC); therefore three different grid spacing are used: 27 km, 9 km, and 3 km. Each simulation is run as a single nest with 45 vertical levels and with a time step prescribed to preserve numerical stability at each respective grid point spacing.

Varying convective schemes are used by the operational models, which suggests that convective initiation may be more dependent on the effects of parameterized convection than on a specific scheme in this case. Therefore, three different convective parameterizations are used in the series of

simulations conducted for this study. At 27 km, separate simulations are run with the Kain-Fritsch (KF; Kain 2004, Kain and Fritsch 1990, 1993), Betts-Miller-Janjic (BMJ; Janjic 1994, 2000), and Grell (Grell and Devenyi 2002) convective schemes. Grell and Devenyi (2002) provides the only scheme available in the WRF-ARW that is recommended for simulations with a grid point spacing less than 10 km, thus only one simulation is run at 9 km using the Grell convective parameterization. Due to the high temporal and spatial resolution of the 3 km simulation, convective processes can be treated explicitly and a convective parameterization is not required. Overall, five simulations are conducted for this study: 27 km with the KF scheme, 27 km with the BMJ scheme, 27 km with the Grell scheme, 9 km with the Grell scheme, and 3 km with explicit convection.

Other model physics and dynamics are set at the default values for the WRF-ARW. The boundary layer parameterization used is the Yonsei University (YSU; Skamarock et al. 2005) scheme, the microphysics scheme is a single moment, five phase parameterization (Lin et al. 1983), and the surface physics are prescribed by the Noah Land Surface Model (Chen and Dudia 2001). These simulations include non-hydrostatic dynamics with 3rd order Runge-Kutta time integration, 5th order horizontal advection, and 3rd order vertical advection. The lateral boundary conditions are provided by the NARR and Rayleigh damping is used in the vertical over the top 5000 meters of the domain.

To analyze the results, model output is converted to GEMPAK (DesJardin 1991) files and analyzed via several gridded data and point data plotting programs. Model output is first examined from a synoptic standpoint in order to verify 1) consistency between simulations, and 2) similarity to the actual evolution of the case study. Total precipitation accumulation and model-derived convective precipitation are examined to determine whether or not deep convective initiation occurs in each of the model simulations, plan views of most unstable convective available potential energy (MUCAPE) and surface convective inhibition (CIN) are plotted for analysis of the favorability of the atmosphere for convective initiation, and model soundings are analyzed to inspect the overall evolution of the thermodynamic profile from the standpoint of atmospheric stability, particularly at low levels. For a deeper understanding of how the capping inversion responds to convective parameterization, both the stability tendency (Bluestein 1993):

$$\frac{\partial}{\partial t}\left(-\frac{\partial \theta}{\partial p}\right) = -\frac{\partial}{\partial p}\left(-\mathbf{v}\cdot\nabla_{\mathrm{p}}\theta\right) - \omega\frac{\partial}{\partial p}\left(-\frac{\partial \theta}{\partial p}\right) - \delta\frac{\partial \theta}{\partial p} - \frac{\partial}{\partial p}\left(\frac{\theta}{C_p T}\frac{dQ}{dt}\right)$$

and the temperature tendency (Bluestein 1993):

$$\frac{\partial T}{\partial t} = -\mathbf{v}\cdot\nabla_{\mathrm{p}}T + \omega\sigma\frac{p}{R}$$

are plotted in the layer of the strongest low-level temperature inversion; in this case, at 800 hPa. These tendencies are then compared to the behavior of the capping inversion at that level in order to separate the effects of parameterized convection versus the physical and dynamic responses of the atmosphere.

3. Results

A synoptic analysis of each simulation reveals a striking similarity between all WRF-ARW simulations, as well as between these simulations and the actual evolution of

the case study. While the dryline progresses slightly faster in the WRF simulations than in reality, the overall placement of the low pressure system and associated fronts closely resembles observed conditions on 22 October 2004. All simulations run at 27 km produce similar results, thus the 27 km simulation run with the KF scheme is chosen as a representative simulation for all 27 km runs. Precipitation is produced at the surface in all simulations with parameterized convection (Figures 4 and 5) and is not produced with explicit convection (Figure 6). When plotting only convective precipitation (not shown), the precipitation produced along the dryline in northwest Iowa is identified as convective. All simulations produce shallow convection, which is reflected in model soundings.

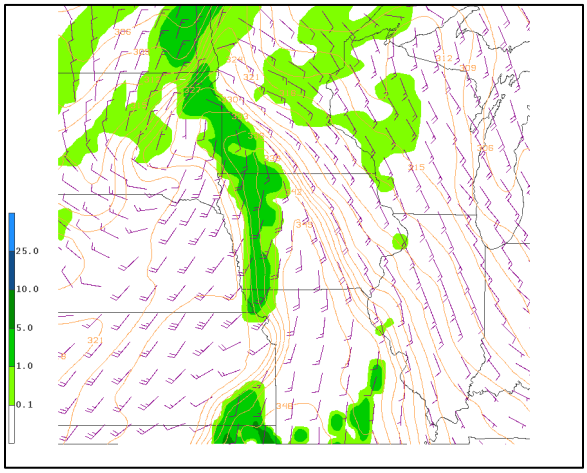

Figure 4. 27 km simulation at 20 UTC 22 October 2004. Shading is 1-h precipitation in mm and contours are equivalent potential temperature at a 2 K interval at 950 hPa. Half wind barbs are 2.5 m s^{-1} and whole wind barbs are 5 m s^{-1} at 10 m.

Environmental soundings taken ahead of the dryline before precipitation is produced at the surface show the presence of a substantial capping inversion around 800 hPa, which is accompanied by a layer of dry air. Between 1800 and 1900 UTC 22 October, significant cooling and some moistening of the 800 hPa level occurs in both the 27 km and 9 km simulations (Figures 7 and 8), which works to decrease the capping inversion and allow deep convection to initiate. Despite a cooling and moistening trend observed at 800 hPa in the 3 km simulation, the overall trend is not a cooling and moistening of the air as is seen in the other simulations; instead, the boundary layer is lifting and almost eliminating instability (Figure 9).

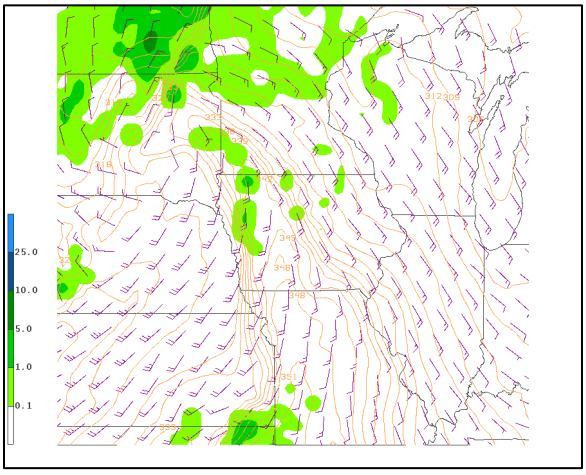

Figure 5. As in Figure 4, but for the 9 km simulation.

Examination of the instantaneous temperature tendency at 800 hPa for 1800 UTC reveals that the atmosphere should be trending toward warmer temperatures ahead of the dryline in the 27 km and 9 km simulations (Figures 10 and 11), but is consistent with the cooling observed at 800 hPa in the 3 km simulation (Figure 12). Instantaneous stability tendency at 800 hPa for 1800 UTC also indicates increasing stability ahead of the dryline for all simulations, which is inconsistent with the 27 km and 9 km simulations, but consistent with the 3 km simulation (Figures 13-15). From a dynamic standpoint, all simulations should be trending towards higher stability,

which would prevent deep convective initiation.

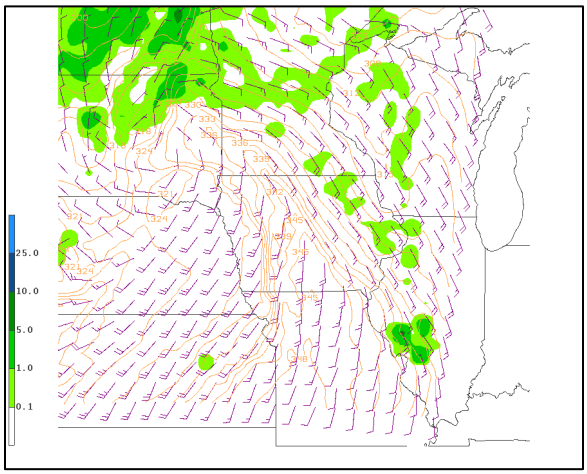

Figure 6. As in Figure 4, but for the 3 km simulation.

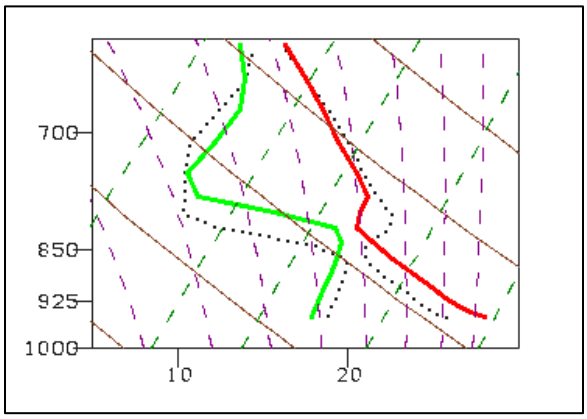

Figure 7. Environmental soundings for 18 UTC (dotted) and 19 UTC (solid colored) for the 27 km simulation.

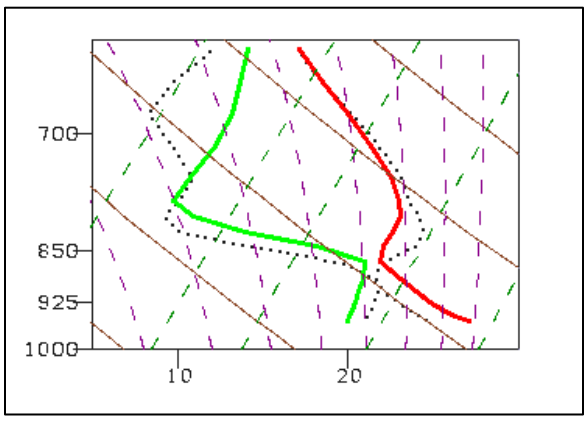

Figure 8. As in Figure 7, but for the 9 km simulation.

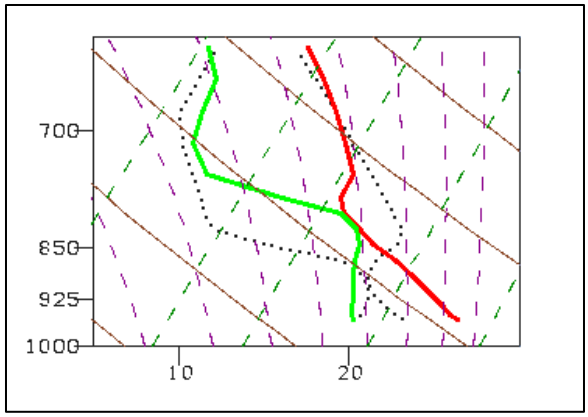

Figure 9. As in Figure 7, but for the 3 km simulation.

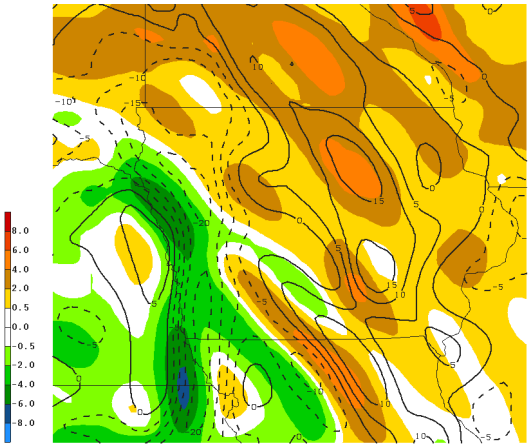

Figure 10. 27 km simulation at 20 UTC 22 October 2004. Shading is the computed instantaneous temperature tendency at 800 hPa at 18 UTC in K s^{-1}, scaled by 10^4. Contours are temperature change at 800 hPa from 18 UTC to 19 UTC in K, scaled by 10^1. Dashed lines (cool shading) indicate cooling.

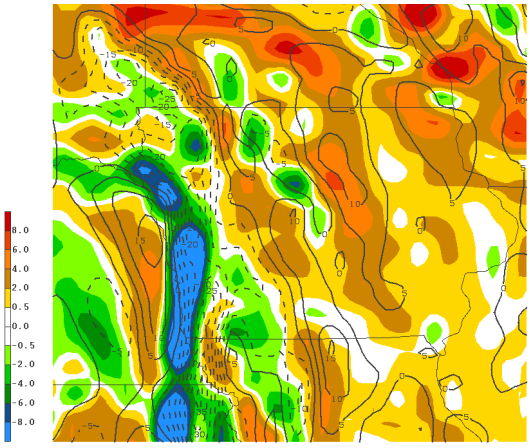

Figure 11. As in Fig. 10, but for the 9 km simulation.

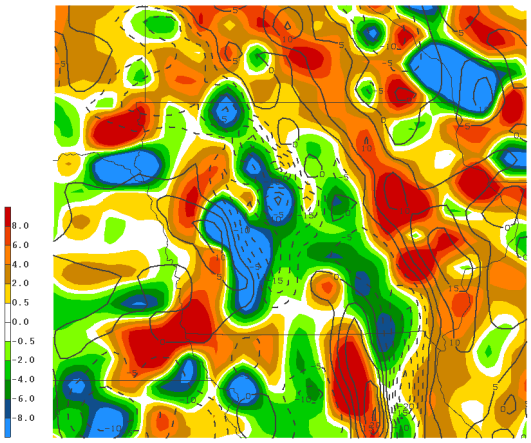

Figure 12. As in Fig. 10, but for the 3 km simulation.

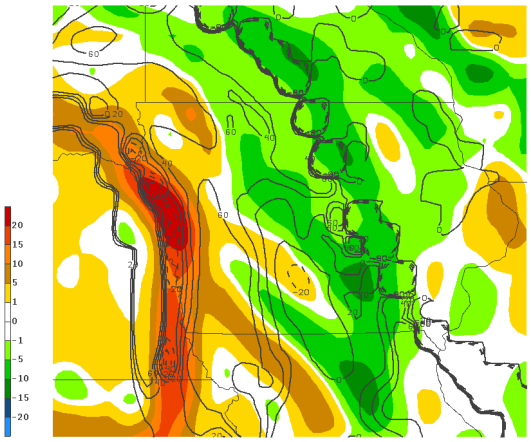

Figure 13. 27 km simulation at 20 UTC 22 October 2004. Shading is computed instantaneous stability tendency at 800 hPa at 18 UTC in K s^{-1} Pa^{-1}, scaled by 10^8. Contours are the difference of surface CIN at 19 UTC and CIN at 18 UTC in J kg^{-1}. Solid lines (cool colors) indicate decreasing stability.

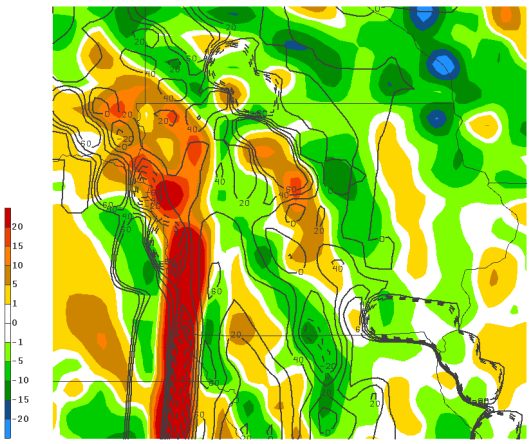

Figure 14. As in Fig. 13, but for the 9 km simulation.

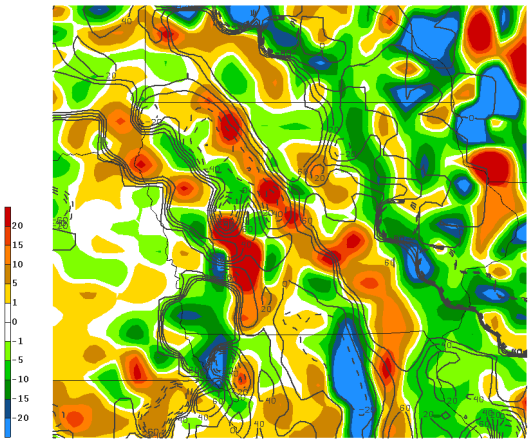

Figure 15. As in Fig. 13, but for the 3 km simulation.

4. Discussion and Conclusions

From these results, it appears that the effect of parameterized convection is to decrease convective inhibition present in the low levels by cooling the capping inversion, as well as moistening that layer. While the tendencies of the atmosphere point to a strengthening cap ahead of the dryline, the opposite result occurs, which points to an effect that is not accounted for by the tendency equations.

Shallow convective schemes in cloud-resolving numerical models are activated when all the conditions for convective initiation are met except the minimum cloud depth (Kain 2004). The overall effect of the shallow convective parameterization is to mix cooler air downward and moisture upward, which decreases convective inhibition by eliminating the capping inversion. It is important to note that the purpose of a convective parameterization is to eliminate instability in the model, not to produce realistic precipitation at the surface. Shallow convective schemes work to eliminate low level stability so that deep convection can be initiated, thus eliminating deep layer instability and resulting in precipitation accumulation at the surface.

Therefore, the inclusion of a convective parameterization in model simulations may produce deep convection more often than is observed in highly capped environments.

While these conclusions are based on a single case, the operational utility of a high-resolution model with explicit convection is demonstrated in this study. Disagreement in the occurrence of deep convection between models run with parameterized convection and a model which treats convection explicitly may indicate a need for further investigation of the stability tendency, especially in the presence of high CIN. In an operational setting, forecasters should be aware of model-produced decreasing temperatures and increasing moisture within the shallow cloud layer, and check for consistency with temperature and moisture advection.

In the future, additional simulations will be run which change the boundary layer parameterization in order to isolate the different roles that parameterizations may have on convective initiation. In addition, other cases will be examined to gain a better understanding of convective initiation in both parameterized and explicit convection models.

5. Acknowledgements

The authors thank the staff of WFO Sioux Falls for their input and reviews throughout the duration of this study.

6. References

Chen, F. and J. Dudhia, 2001: Coupling an advanced land-surface/hydrology model with the Penn State/NCAR MM5 modeling system. Part II: Preliminary model validation, *Mon. Wea. Rev.*, **129**, 587-604.

Grell, G. A., and D. Devenyi, 2002: A generalized approach to parameterizing convection combining ensemble and data assimilation techniques. *Geophys. Res. Lett*, **29**.1693, doi:10.1029/2002GL015311

Janjic, Z. I., 1994: The step-mountain eta coordinate model: Further developments of the convection, viscous sublayer, and turbulence closure schemes. *Mon. Wea. Rev*., **122**, 927-945.

Janjic, Z. I., 2000: Comments on "development and evaluation of a convection scheme for use in climate models." *J. Atmos. Sci.*, **57**, 3686.

Kain, J. S., 2004: The Kain-Fritsch convective parameterization: an update. *J. Appl. Meteor.*, **43**, 170-181.

Kain, J. S. and J. M. Fritsch, 1990: A one-dimensional entraining/detraining plume model and its application in convection parameterization. *J. Atmos. Sci*., **47**, 2784-2802.

Kain, J. S. and J. M. Fritsch, 1993: Convective parameterization for mesoscale models: The Kain-Fritsch scheme. *The Representation of Cumulus Convection in Numerical Models, Meteor. Monogr*., No. 24, Amer. Meteor. Soc, 165-170.

Lin, Y. L., R. D. Farley, and H. D. Orville, 1983: Bulk parameterization of the snowfield in a cloud model. *J. Climate Appl. Meteor.*, **22**, 1065-1092.

Mesinger, F., Coauthors, 2006: North American Regional Reanalysis. *Bull. Amer. Meteor. Soc.*, **87**, 343-360.

Skamarock, W. C., J. B. Klemp, J. Dudhia, D. O. Gill, D. M. Barker, W. Wang, and J. G. Powers, 2005: A description of the advanced research WRF version 2. NCAR Tech. Note 468+STR, 88 pp.